Pervasive Arctic lead pollution suggests substantial growth in medieval silver production modulated by plague, climate, and conflict

Joseph R. McConnell[a,1], Nathan J. Chellman[a], Andrew I. Wilson[b,c], Andreas Stohl[d], Monica M. Arienzo[a], Sabine Eckhardt[d], Diedrich Fritzsche[e], Sepp Kipfstuhl[f], Thomas Opel[e], Philip F. Place[g], and Jørgen Peder Steffensen[h]

[a]Division of Hydrologic Sciences, Desert Research Institute, Reno, NV 89512; [b]Faculty of Classics, University of Oxford, Oxford OX1 3LU, United Kingdom; [c]Institute of Archaeology, University of Oxford, Oxford OX1 2PG, United Kingdom; [d]Department of Atmospheric and Climate Research, Norwegian Institute for Air Research, N-2027 Kjeller, Norway; [e]Polar Terrestrial Environmental Systems, Alfred-Wegener-Institut Helmholtz-Zentrum für Polar-und Meeresforschung, 14473 Potsdam, Germany; [f]Glaciology, Alfred-Wegener-Institut Helmholtz-Zentrum für Polar-und Meeresforschung, 27570 Bremerhaven, Germany; [g]Earth and Environmental Sciences, University of Rochester, Rochester, NY 14627; and [h]Centre for Ice and Climate, University of Copenhagen, DK-1017 Copenhagen, Denmark

Edited by Eric W. Wolff, University of Cambridge, Cambridge, United Kingdom, and accepted by Editorial Board Member A. R. Ravishankara June 13, 2019 (received for review March 15, 2019)

Lead pollution in Arctic ice reflects large-scale historical changes in midlatitude industrial activities such as ancient lead/silver production and recent fossil fuel burning. Here we used measurements in a broad array of 13 accurately dated ice cores from Greenland and Severnaya Zemlya to document spatial and temporal changes in Arctic lead pollution from 200 BCE to 2010 CE, with interpretation focused on 500 to 2010 CE. Atmospheric transport modeling indicates that Arctic lead pollution was primarily from European emissions before the 19th-century Industrial Revolution. Temporal variability was surprisingly similar across the large swath of the Arctic represented by the array, with 250- to 300-fold increases in lead pollution observed from the Early Middle Ages to the 1970s industrial peak. Superimposed on these exponential changes were pronounced, multiannual to multidecadal variations, marked by increases coincident with exploitation of new mining regions, improved technologies, and periods of economic prosperity; and decreases coincident with climate disruptions, famines, major wars, and plagues. Results suggest substantial overall growth in lead/silver mining and smelting emissions—and so silver production—from the Early through High Middle Ages, particularly in northern Europe, with lower growth during the Late Middle Ages into the Early Modern Period. Near the end of the second plague pandemic (1348 to ∼1700 CE), lead pollution increased sharply through the Industrial Revolution. North American and European pollution abatement policies have reduced Arctic lead pollution by >80% since the 1970s, but recent levels remain ∼60-fold higher than at the start of the Middle Ages.

ice core | lead pollution | Arctic | plague | Middle Ages

Lead measured in Arctic (1–6) and Alpine (7–9) ice cores has been used to document changes in atmospheric lead pollution from ancient European mining and smelting as well as recent fossil fuel combustion and other industrial activities, and to infer historical and economic implications. Close linkages to ancient economies are expected, in part, because silver used in coinage such as the Roman *denarius* largely derived from lead-rich galena ores and because lead was used extensively in the metallurgical extraction of silver (10). In one recent study (2), pollution deposition measured in a central Greenland ice core was used to reconstruct annual European lead emissions from ancient mining and smelting activities from 1000 BCE to 800 CE and document parallel declines in Greenland lead pollution and the silver content of Roman *denarii* during the second and third centuries. This record showed that increases in lead emissions during antiquity were associated closely with periods of prosperity, and decreases were associated with periods of economic disruption. Low levels, especially during the last decades of the Roman Republic, and 4-fold higher levels during the Pax Romana at the apogee of the Roman Empire indicated substantial economic growth during the latter period. Particularly striking were pronounced and lasting declines during the second-century Antonine Plague and third-century Plague of Cyprian, suggesting low societal resilience to pestilence. Here we used high-depth–resolution measurements (Fig. 1) in an array of accurately dated ice cores located between longitudes 56°W and 95°E and spanning nearly half the Arctic (*SI Appendix*, Fig. S1) to extend analysis of Arctic lead pollution and European economic history to include the Middle Ages, Early Modern Period, and Modern Period. Using state-of-the-art atmospheric transport and deposition modeling to determine probable lead pollution provenance, as well as comparisons to historical information, including economic proxies such as European grain prices (11) and tree fellings from historical construction timber (12), we evaluated Arctic pollution growth rates and possible drivers of observed annual to centennial changes in pollution such as climate variations, major wars, and plagues, as well as exploitation and exhaustion of new mining areas.

We measured a range of elements and chemical species, including lead and the mineral dust indicator cerium, in a broad

Significance

Detailed lead pollution measurements in an array of 13 ice cores spanning nearly half the Arctic showed surprisingly similar temporal variability during the past 2 millennia until the Industrial Revolution. Lead pollution increased by 250- to 300-fold from the Early Middle Ages to the 1970s industrial peak, reflecting large-scale emissions changes from ancient European silver production, recent fossil fuel burning, and other industrial activities. Pronounced decadal-scale increases coincided with exploitation of new mining districts, technology development, and periods of economic prosperity, while decreases coincided with climate disruptions, famines, major wars, and plagues. Despite midlatitude pollution abatement policies that reduced Arctic lead pollution by >80% since the 1970s, recent levels remain 60-fold higher than at the start of the Middle Ages.

Author contributions: J.R.M. designed research; J.R.M., N.J.C., A.S., M.M.A., S.E., D.F., S.K., T.O., P.F.P., and J.P.S. performed research; J.R.M., N.J.C., A.I.W., and A.S. analyzed data; and J.R.M., N.J.C., A.I.W., and A.S. wrote the paper.

The authors declare no conflict of interest.

This article is a PNAS Direct Submission. E.W.W. is a guest editor invited by the Editorial Board.

[1]To whom correspondence may be addressed. Email: Joe.McConnell@dri.edu.

This article contains supporting information online at www.pnas.org/lookup/suppl/doi:10.1073/pnas.1904515116/-/DCSupplemental.

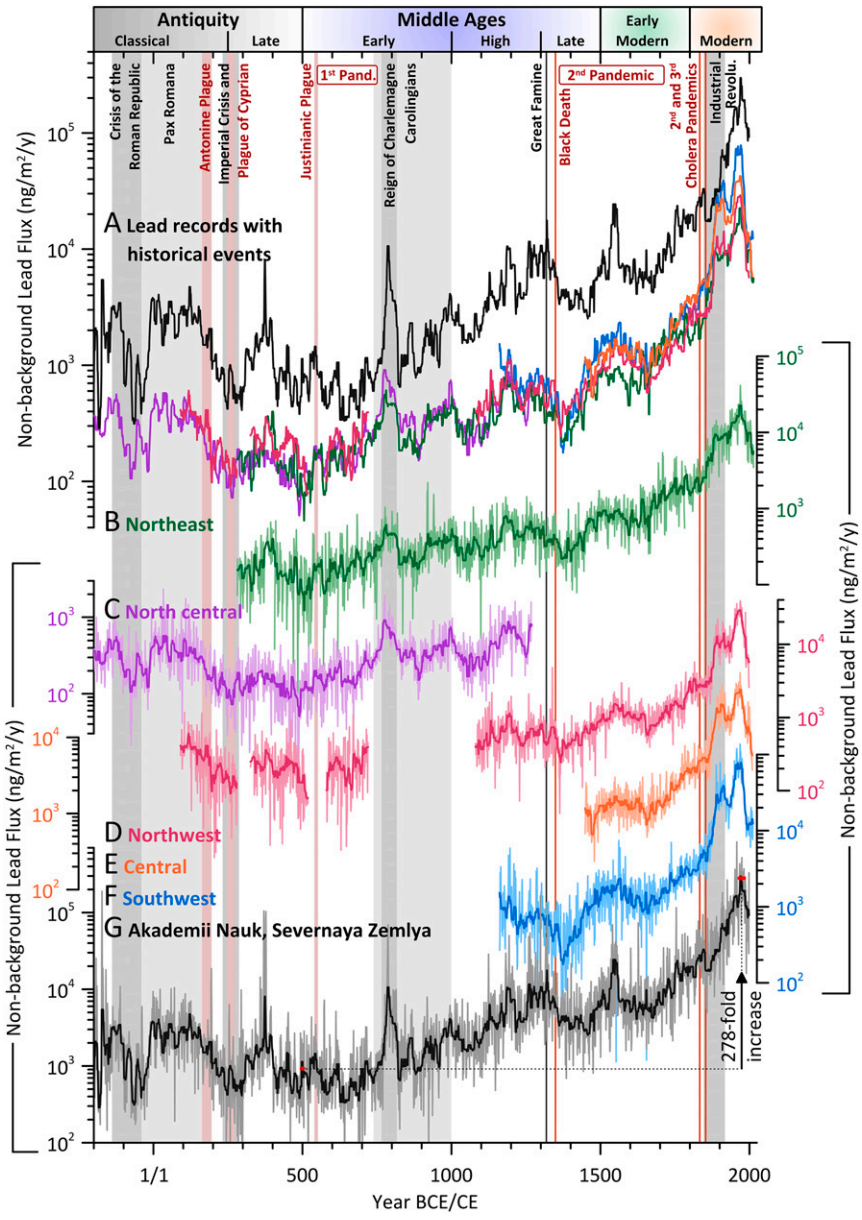

Fig. 1. Annual lead pollution deposition during the past 2,200 y documented in an array of ice cores spanning nearly half the Arctic, including 12 ice cores from Greenland and 1 from Severnaya Zemlya in the Russian Arctic (*SI Appendix*, Fig. S1). (*A*) Median filtered (11-y) AN record from Severnaya Zemlya and Greenland regional composite records (records and colors same as in *B*–*G*) on the same logarithmic scale. (*B*–*F*) Individual Greenland regional composites (annual and 11-y median filtered values shown with thin and thick lines, respectively). (*G*) AN record from Severnaya Zemlya. The individual Greenland ice core records (*SI Appendix*, Fig. S1 and Table S1) were grouped by location and regional records of annual concentration (*SI Appendix*, Fig. S2), flux, and enrichment (*SI Appendix*, Fig. S3) were computed as the geometric mean of the individual ice core records. The ACT2 (4) and the 200 BCE to 800 CE part of the NGRIP2 (2) record have been published previously (*SI Appendix*, Table S1). Measurements in the few previously reported Arctic lead measurements (3–5), all confined to the central region of the Greenland ice sheet, are consistent with the records presented here (*SI Appendix*, Fig. S2). Because accurate dating of ice core records is critical for meaningful historical interpretation, all cores were volcanically synchronized to an accurately dated Arctic reference record (*Materials and Methods*). Uncertainties in the individual core chronologies were estimated to be <2 y (2) for the Greenland records and <5 y for the AN core (*Materials and Methods*). Widespread pollution increased more than 250-fold from the Early Middle Ages to 1970s, with sharp, often sustained increases coincident with periods of political stability (e.g., early Carolingian Empire) and exploitation of new mining regions, and decreases coincident with plagues (e.g., Black Death, second plague pandemic from 1348 to ~1700 CE; second cholera pandemic from 1829 to 1837 CE; third cholera pandemic from 1846 to 1860 CE), climate (e.g., Little Ice Age), major wars, and other externalities. Similar variability throughout the Arctic array indicates large-scale, common changes in lead emissions.

array of 13 Arctic ice cores with the continuous ice core analytical system at the Desert Research Institute (DRI) (13), using previously established methods for ice core dating and nonbackground or pollution lead determinations (*Materials and Methods*) (2, 14). Annual records from similar geographic regions were combined into composite records representative of specific regions of Greenland, in addition to the Akademii Nauk (AN) record from Severnaya Zemlya representative of the Russian Arctic (Fig. 1). Despite large differences in site characteristics, including elevation and snowfall rate (*SI Appendix*, Table S1), the magnitude of change in lead pollution deposition in Greenland was similar across all regional composites during the past 2 millennia before the Industrial Revolution (Fig. 1 and *SI Appendix*, Figs. S2 and S3). Depositional flux ranged from ~100 ng/m^2/y in late antiquity and the Early Middle Ages to ~26,000 ng/m^2/y at the peak of modern industrial emissions in the early 1970s before implementation of pollution abatement policies such as the US Clean Air Act of 1970—a more than 250-fold increase in Arctic lead pollution. Compared with the Greenland records, flux generally was an order of magnitude higher in the AN record, with even larger overall changes. These increases were equivalent to an average growth rate in Arctic lead pollution of ~0.38%/y from 500 CE to the 1970s industrial peak. Although potentially influenced by local emissions sources, ~200-fold increases in total lead deposition were reported during approximately this same period in a Swiss peat bog core (15). Superimposed on these long-term exponential increases were multiannual to multidecadal periods of rapid, 2- to 10-fold increases and decreases that occurred simultaneously throughout the Arctic array, indicating synchronous, large-scale changes in midlatitude lead emissions.

Unlike paleoenvironmental records from Alpine ice (7–9), peat bog (15), or lake sediment cores (16) located within Europe and potentially influenced by local emissions (17), records from the remote Arctic are far removed from emissions sources and so reflect regional- to continental-scale emissions (2). To quantify long-range transport over thousands of kilometers and underpin investigation of these rapid changes by identifying probable sources of Arctic lead pollution, we used the FLEXPART atmospheric transport and deposition model (18, 19) (*Materials and Methods*). For comparison, the 3 north Greenland and the central and southwest Greenland regional records subsequently

were combined into North Greenland (NG) (Fig. 2) and South Greenland (SG) composite records, respectively (*SI Appendix*, Fig. S4). The FLEXPART emissions sensitivity maps (*SI Appendix*, Fig. S5) were combined similarly (*SI Appendix*, Fig. S6). The AN/NG sensitivity ratio (Fig. 3) shows that AN was 2- to 12-fold more sensitive than the NG composite to European emissions—consistent with the ∼8-fold higher deposition seen in the AN ice core record during the last 2 millennia before the Industrial Revolution (Figs. 1 and 4)—indicating that the dominant sources of Arctic pollution were European. Archaeological evidence indicates potential emissions from sites in modern southern China during the Middle Ages (20, 21), but the model simulations (Fig. 3) show that 1) sites in the Arctic array are 1 to 2 orders of magnitude less sensitive to such emissions and 2) the AN/NG sensitivity ratio to emissions from China is close to 1, which is inconsistent with the ∼8-fold higher deposition observed at AN. Therefore, we interpret the Arctic records as representative of overall European emissions, recognizing that sensitivity was higher to northern European emissions and that the NG record is biased toward western Europe and AN is biased toward eastern Europe (Fig. 3). We evaluated growth (*Materials and Methods*) rates (Fig. 2) and shorter-term variations (Fig. 4) in Arctic lead pollution from 500 CE to present during different historical periods.

Early Middle Ages: 500 to 1000 CE

Average lead pollution growth rates were similar, with 0.20(±0.01 1σ)%/y measured in the NG record and 0.27(±0.01)%/y measured in AN (Fig. 2 and *SI Appendix*, Table S2). A relatively long period of sustained pollution increase began *ca*. 625 CE and lasted through 1000 CE. The early part of this period corresponded to the establishment of mining and smelting activities at Melle in western France, exploited from 602 to *ca*. 1000 CE (22). A rapid, 4- to 6-fold increase *ca*. 740 to 785 CE from a low point, especially after 750 CE, partly coincides with the establishment in 751 CE of a mint at Melle under Pepin I, suggesting substantial silver production at the site at that time; it functioned as the Carolingian mint under Charlemagne (768 to 814 CE), where his "Aachen penny" was struck. This 45-y period of anomalously high Arctic lead pollution was the first time that sustained Arctic lead pollution exceeded levels during the Pax Romana at the apogee of the Roman Empire. Another indicator of economic prosperity, tree felling rates from dendrochronologically dated construction timber indicative of new construction in Germany and France (23), also reached a similar short-term peak soon afterward (Fig. 4). After the end of Charlemagne's reign in 814 CE, pollution sharply declined from *ca*. 815 to 835 CE (Fig. 1). The final part

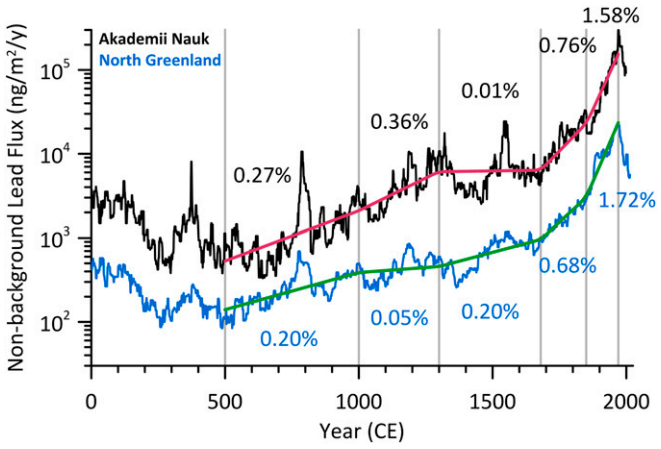

Fig. 2. Arctic lead pollution (11-y median filter) with fitted average growth rates (*Materials and Methods*) during specific historical periods in the NG (green) and AN (red) records (*SI Appendix*, Table S2).

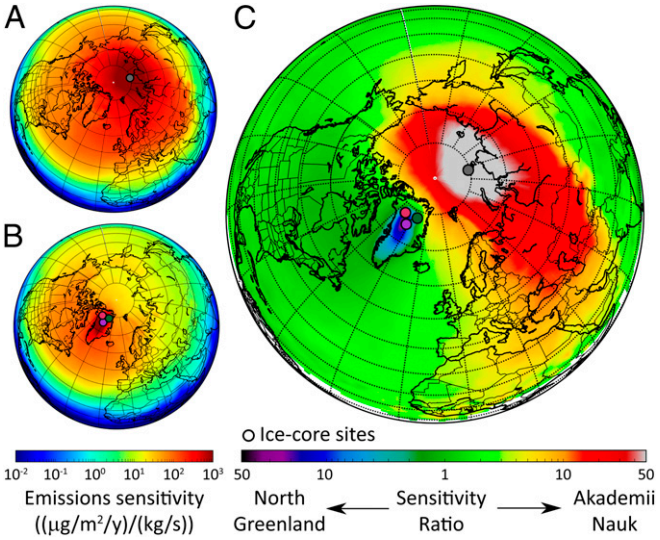

Fig. 3. FLEXPART (18, 19) simulation-based sensitivity of the (*A*) AN and (*B*) NG ice core records to lead emissions and (*C*) their ratio. The ∼8-fold higher lead deposition observed in the AN record compared with the NG composite (Fig. 1) is consistent with the 2- to 12-times higher sensitivity to European emissions in the AN/NG ratio, indicating that lead pollution in the Arctic array was dominated by European emissions before the Industrial Revolution.

of the 45-y pollution high also coincided with increased mining and smelting around Wirksworth (Derbyshire, England) from *ca*. 780 to 855 CE (ref. 24, p. 516), and FLEXPART simulations showed that both ice core records were more sensitive to these emissions. The AN/NG ratio of FLEXPART emissions sensitivities for the early medieval sites at Melle and Wirksworth were comparable (*SI Appendix*, Fig. S1), preventing discrimination between the 2 sources, but lower than for the emissions sites in Germany or elsewhere in northern Europe. In addition, the AN/NG ice core lead flux ratio during the sharp increase from 770 to 815 CE was similar to that during the Pax Romana, suggesting that these emissions came from within the area of the former Roman Empire. Taken together, the ice core and FLEXPART ratios suggest that the sources were mainly in northwestern Europe.

The overall increase in lead pollution from 500 to 1000 CE approximately paralleled European precipitation and temperature trends (Fig. 4), with higher mining and smelting activity coinciding with progressively wetter and warmer conditions later, following the end of the Late Antique Little Ice Age in the second half of the seventh century (23). Short-term periods of particularly low pollution around 835 CE and from 875 to 905 CE coincided with declines in precipitation, and were followed by a century-long period of pollution growth to a distinct maximum at 1000 CE (Fig. 4) that may reflect the discovery and exploitation in 968 CE of rich new lead/silver deposits at Rammelsberg in the Harz Mountains in Germany (24, 25). This first production cycle in the Harz region mines ended between 1002 and 1016 CE, when famine and pestilence resulted in abandonment and flooding of the mines (ref. 24, pp. 566–567), coincident with an immediate and persistent decline in the AN record.

High Middle Ages: 1000 to 1300 CE

Pollution trends in the NG and AN records diverged in the High Middle Ages, with average growth rates declining to 0.05(±0.02)%/y in NG while increasing to 0.36(±0.03)%/y in AN (Fig. 2), probably reflecting the development of mining in Germany that had a greater impact on the AN record (Fig. 3). The second production cycle in the Harz Mountains (*ca*. 1020 to 1077 CE) appears relatively unimportant in our record, but lead peaks in the 12th century coincided with the third Harz production cycle from 1125 to 1181 CE and the first exploitation of the Freiberg/Meissen mines from 1171 to 1188 CE (ref. 24, pp. 694–695). There was a drop thereafter

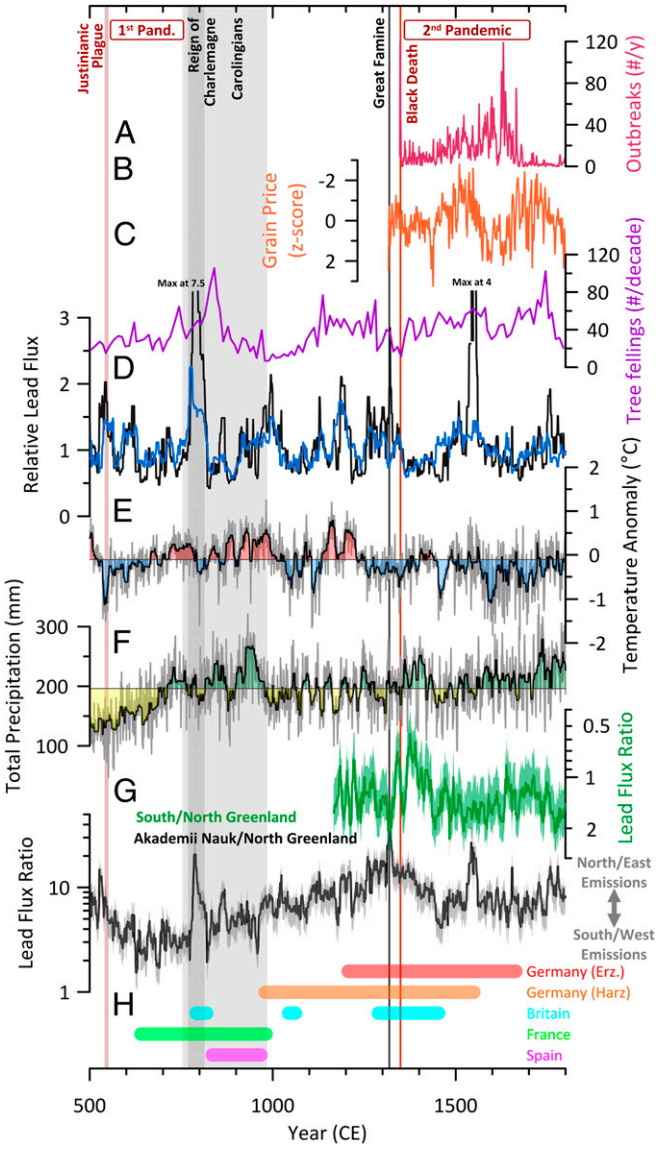

Fig. 4. Arctic lead pollution compared with indicators of plague, economic conditions, and climate from 500 to 1800 CE: (*A*) number of plague outbreaks per year (29), (*B*) average European grain prices (11), (*C*) tree fellings per decade from historical construction timbers (12), (*D*) relative lead pollution flux in NG (blue) and AN (black) calculated by subtracting a 600-y spline fit from the log-transformed deposition records, (*E* and *F*) reconstructed north central European (*E*) temperature anomaly (41) and (*F*) precipitation (23), (*G*) SG/NG and AN/NG lead flux ratios, and (*H*) approximate locations and periods of known medieval and Early Modern mining activity.

from 1202 to 1212 CE as warfare between Staufer and Welf factions ravaged the Harz region, with a nadir between 1203 and 1206 CE when Otto the Welf destroyed the smelteries around Goslar (ref. 24, p. 695). The next major peak in the Arctic lead pollution from *ca*. 1256 to 1307 CE closely followed a silver mining boom from 1254 to 1306 CE, particularly in Bohemia and Hungary (ref. 26, p. 934).

The highest overall pollution levels during the Early and High Middle Ages occurred during the late eighth century and at the beginning and end of the 13th century (Fig. 2), but declines in the NG record indicate that lead/silver mining and smelting emissions, and possibly general economic conditions in much of Europe, already were declining well before the 1300 CE start of the Crisis of the Late Middle Ages.

Late Middle Ages to Late Second Plague Pandemic: 1300 to 1680 CE

Pollution trends during the Late Middle Ages and through the late second plague pandemic were very different in the NG and AN records. Average growth rates in the NG record increased to 0.20(±0.02)%/y. The strong growth observed in the AN record during the Early and High Middle Ages came to an abrupt halt *ca*. 1325 CE, with average growth rates from 1300 to 1680 CE declining to 0.01(±0.04)%/y (Fig. 2).

Consistent with other economic indicators, including average European grain prices and tree felling rates for construction timber (12, 23), periods of decline in lead pollution began early in the 14th century probably as a result of societal problems, climate change and increasing famine in parts of Europe at the onset of the Little Ice Age decades before the pronounced, sharp, Black Death-related decrease about 1350 CE observed throughout the Arctic array. Lead pollution in the NG record declined from 1349 to 1360 CE toward a minimum that lasted (with brief and unsustained increases *ca*. 1391 and 1402) for a century from *ca*. 1348 to 1448 CE. This undoubtedly was the result of the Black Death (bubonic plague) which killed perhaps a third of the population of medieval Europe, massively reducing both the labor force to produce metals, and the demand for them. Lead pollution dropped 50% or more throughout the array (Figs. 1 and 4), with immediate coincident declines largest in the southwest Greenland composite (Fig. 1 and *SI Appendix*, Fig. S4) that was most sensitive to emissions from southern and western Europe (*SI Appendix*, Fig. S5). Declines were short-lived in all Greenland records, with minima *ca*. 1368 CE, 20 y after the arrival of the plague in Europe; the recovery in these records was probably the result of emissions from mines in England and Wales. Declines were much longer-lived in the AN record (more sensitive to German emissions) which did not show renewed pollution growth until more than a century later (Fig. 4).

During the mid- to late-15th century (Fig. 4), lead pollution in both the NG and AN records increased to a distinct maximum between 1530 and 1555 CE. The increase between the mid-15th century and the mid-16th century almost certainly reflected the revival of silver mining in the Erzgebirge and Harz Mountains led by Saxon miners (27); in the late 1450s new developments in mine drainage allowed deeper mining, leading to a revival of work in mines previously considered to be exhausted because of flooding. In the late 1400s, new mines opened up in Saxony and Bohemia, and in 1516 a large and important new mine was discovered at Joachimsthal (the silver coins called "thalers" are an abbreviation of Joachimsthaler, as much of the silver was made into coinage). Technical advances in mining during the course of the 16th century increased output, and Georgius Agricola's treatise *De Re Metallica*, published in 1556 (28), reflected the new interest and revival of silver mining. This 16th-century peak was followed by a century-long, 25% decrease in pollution from *ca*. 1560 until *ca*. 1675 CE in parallel with increased plague outbreaks (29). From the 1580s to 1650 CE, pollution deposition fluctuated between levels equivalent to the lows of the 1580s and the peaks of the late 1400s and early 1500s; even though the pollution during this period was substantially lower than in the 1520s to 1560s, it was well above the levels of the 11th to 12th centuries and the post-Black Death low from 1349 to 1448. The Thirty Years War (1618 to 1648 CE), known to have disrupted mining and the central European economy, coincided with a dip in both the NG and AN records (Fig. 1 and *SI Appendix*, Fig. S4).

The pollution record from 1440 to 1675 thus appears to reflect the recovery of mining in the mid-15th century leading to a 16th-century boom that was modulated by effects of war and the plague, with temporary drops in pollution coinciding with the years of known severe plague resurgences.

Late Second Plague Pandemic to Industrial Revolution: 1680 to 1850 CE

Growth in Arctic lead pollution accelerated after the end of the second plague pandemic and coincident with broader European

economic recovery and technological developments (Fig. 4), with average overall rates jumping from 0.20(±0.02) to 0.68(±0.04)%/y in the NG record and from 0.01(±0.04) to 0.76(±0.07)%/y in the AN record (Fig. 2). In the Derbyshire mines to which both records are particularly sensitive, the later 17th century saw increases in production from improved drainage techniques and expansion in the use of gunpowder for blasting (30). Growth was sustained throughout this 170-y period, with no large or persistent declines documented in either record until *ca*. 1840 CE in the NG record and *ca*. 1850 CE in the AN record (Fig. 2), when periods of relatively minor decline coincided approximately with the second and third cholera pandemics in Europe (31), and, perhaps more importantly, with the economic crises of the mid- to late-1840s which preceded the 1848 revolutions (32).

Industrial Revolution to the Maximum: 1850 to 1970 CE

Increases in Arctic lead pollution growth during the 120 y following the start of the Industrial Revolution *ca*. 1850 CE were pronounced relative to the previous 170 y, in part because of substantial emissions from widespread fossil fuel burning of coal and leaded gasoline used from the early 1940s to the 1970s and 1980s. Pollution growth rates increased to 1.72(±0.08) and 1.58(±0.13)%/y in the NG and AN records, respectively.

As previously reported for central Greenland (3, 4), in regions of the Arctic strongly influenced by North American emissions, including all of Greenland but especially the southwest and central regions (Fig. 1 and *SI Appendix*, Figs. S4–S6), Arctic pollution rose rapidly from 1850 to 1915 CE as a result of the Industrial Revolution. This was followed by a pronounced drop during the Great Depression and then a rapid rise to the 1970s peak (3, 4). Because of much lower sensitivity to North American emissions, the late 19th-century increase was less pronounced in the AN record, although increases in lead emissions from Soviet-era industries at Norilsk and on the Kola Peninsula (33, 34) and elsewhere in northeastern Europe undoubtedly contributed to pollution in the eastern Arctic during the second half of the 20th century. The 1930s decline during the Great Depression also is largely absent in the AN record.

Conclusion

The array of accurately dated ice core records clearly documents exponential, 250- to 300-fold increases in Arctic lead pollution from the Early Middle Ages to the 1970 industrial peak. Decadal to multidecadal increases and decreases of lead deposition throughout the broad Arctic array indicate common, large-scale changes in European and later North American emissions (*SI Appendix*, Fig. S5). Historically documented mining activity in northern Europe from the Early Middle Ages to the Early Modern Period is precisely reflected in the ice core records. Apart from the marked peak between the 770s and 815 CE, lead pollution sustained over decades at or above the levels of the high Roman Empire only began in the 12th century. However, because of the more northerly location of medieval mining regions to which the coring sites are more sensitive, this does not necessarily mean that the emissions at that time were higher than during the Roman period.

Lead pollution growth during the Early Middle Ages was surprisingly pronounced (Fig. 2), with comparisons to European climate records suggesting that mining and smelting activities, and so silver production, were sensitive to climate stresses and social unrest, particularly during the Early and High Middle Ages. However, comparisons with European plague and economic indicators such as average European grain prices and tree felling rates related to construction (Fig. 4), suggest that decadal- to century-scale changes in Arctic pollution during the second plague pandemic of the Late Middle Ages and Early Modern Period were dominated by the impacts of plague.

Implementation of pollution abatement policies, such as US Clean Air Act of 1970 and similar legislation in other countries, resulted in immediate and pronounced 80% declines in overall Arctic lead pollution by the end of the 20th century. Decreases in industrial emissions associated with economic and political changes in central and eastern Europe and the 1991 dissolution of the Soviet Union probably contributed to the sharp drop in lead deposition in the Russian Arctic as well. Even after recent ∼80% declines, however, modern Arctic lead pollution remains ∼60-fold higher than at the beginning of the Middle Ages.

Materials and Methods

Arctic Ice Core Array. Lead, cerium, and sulfur, in addition to a broad range of other chemical and elemental species, were measured in an array of 13 Arctic ice cores using the continuous ice core analytical system at DRI (4, 13) and previously established methods optimized for pollution lead determinations (2). Included in the array (*SI Appendix*, Table S1) were 12 cores collected at 10 sites primarily in the cold, dry snow zone of the Greenland ice sheet and 1 core collected from the low-elevation AN ice cap on Severnaya Zemlya (35). The array stretched ∼2,200 km west to east from 56°W in northwest Greenland to 95°E in the Russian Arctic, and ∼1,600 km south to north from 66°N to 81°N (*SI Appendix*, Fig. S1).

The DRI ice core analytical system includes 2 Element2, High-Resolution Inductively Coupled Plasma Mass Spectrometers (HR-ICP-MS) and a number of other instruments operating in parallel for continuous, near–real-time measurements of ∼30 elements, chemical species, and isotopes simultaneously. Cores in the Arctic array were measured during a span of 12 y, and protocols evolved during that time. For all cores, one HR-ICP-MS was used in medium-slit resolution to measure a broad range of elements, including indicators of sea salts, marine biogenic emissions, volcanic fallout, and continental dust. Different configurations were used, however, to measure lead in specific cores. For the North Greenland Ice Core Project 2 (NGRIP2), Tunu2013, Summit_2010, Summit_2015, and Eurocore_2015 (a.k.a. Place) cores (*SI Appendix*, Table S1), the second HR-ICP-MS was used in low-slit resolution and electronic scan mode to measure only thallium, lead, and bismuth. Detection limits for lead in this configuration were ∼0.01 pg/g. For all other cores, the second HR-ICP-MS also was used in low-slit resolution, but mass scans included a broad range of elements, from sodium (mass 23) to uranium (mass 238). Detection limits for this configuration were ∼0.07 pg/g. Regardless of which configuration was used, detection limits for lead were <5% of the minimum concentrations of ∼1.4 pg/g measured in the array.

Annual average concentrations of pollution lead were derived from the lead (*SI Appendix*, Fig. S2) and cerium measurements following the same procedures recently used for NGRIP2 (2), including corrections for 1) underrecovery of more recalcitrant cerium (36) and 2) background volcanic emissions. Annual fluxes were determined by multiplying the concentrations by the annual layer thickness approximately corrected for ice flow thinning (2). Lead enrichment relative to crustal dust was calculated from the measured lead and recovery-corrected cerium measurements following standard procedures (*SI Appendix*, Fig. S3). Individual Greenland records were grouped by location into composite regional records of annual concentration (*SI Appendix*, Fig. S2), flux (Fig. 1), and enrichment (*SI Appendix*, Fig. S3), computed as the geometric mean of the contributing individual ice core records. To reduce variability in annual lead deposition from year-to-year changes in long-range atmospheric transport and deposition previously determined from FLEXPART model simulations for NGRIP (2), annual lead pollution records were filtered using an 11-y median filter.

Ice Core Chronologies. Accurate and consistent dating of ice core records is critical for meaningful historical interpretation. Chronologies for many of the Greenland ice cores were reevaluated using volcanic synchronization to an accurately dated Arctic reference record followed by adjustment of the multiparameter, annual-layer-counted age scale as necessary. Volcanic horizons were identified by clear, sharp increases in non–sea-salt sulfur concentrations attributed to explosive volcanism (37) typically with an unambiguous tie point to the reference about every 10 y. The Arctic reference record was comprised of high-time–resolution, accurately dated, non–sea-salt sulfur measurements in the NGRIP2 core from 200 BCE to 1258 CE (2) and the North Greenland Eemian (NEEM)_2011_S1 core from 1259 to 2006 CE (38). Uncertainty in the reference chronology was estimated to be <2 y based on prior comparisons of cosmogenic nuclides concentrations (2), including both high- (38) and low-frequency variations (39) of ^{10}Be in Greenland ice and ^{14}C in tree wood (IntCal13). Uncertainties in the synchronized Greenland records in the array were comparable and estimated to be <2 y.

Because of pervasive summertime surface melting, percolation, and refreezing at the lower-elevation AN site (*SI Appendix*, Table S1), as well as the strong influence of nearby marine biogenic emissions on the sulfur record, synchronization with non–sea-salt sulfur alone was ambiguous, so the AN chronology was determined, instead, using an iterative approach. First, prominent volcanic synchronization points between the AN and Arctic reference record (e.g., fallout from the massive 1783 Icelandic eruption of Laki), 20th-century plutonium increases associated with the thermonuclear testing (40), and a sharp increase in ice core ^{10}Be concentration assigned to 775 CE (38) were used to develop an initial

chronology. Within these constraints, annual layers were identified and counted based primarily on seasonal variations in stable water isotopes. Using this chronology, further volcanic tie points were identified using non–sea-salt sulfur, acidity, and other measurements in AN and the Arctic reference record, followed by revised annual layer counting. The process was repeated until a stable chronology was developed. The final AN chronology was somewhat different from previous AN age scales (35) and uncertainty estimated to be <5 y from 500 to 1999 CE, with <2-y uncertainty at many volcanic tie points determined by the uncertainty in the reference record (2).

Estimated Growth Rates. A continuous, piecewise linear regression was fitted using a nonlinear least-squares function to the log-transformed lead flux with fixed, historically determined breakpoints (Fig. 2) at 500, 1000, and 1300 CE representing the start of the Early, High, and Late Middle Ages, as well as 1680 and 1850 CE representing the late second plague pandemic and start of the second Industrial Revolution. Uncertainties (1σ) on the fitted slopes or growth rates generally were less than 10% (*SI Appendix*, Table S2). Additional simulations (Monte Carlo, $n = 1{,}000$) with random breakpoints distributed within ±25 y of the fixed historically determined breakpoints were used to estimate uncertainties associated with using these specific time constraints (*SI Appendix*, Table S2).

Atmospheric Transport and Deposition Modeling. Long-range transport of lead pollution during the Middle Ages is implicit since ice-coring sites on Severnaya Zemlya and Greenland were located thousands of kilometers from the potential mining and smelting locations (*SI Appendix*, Fig. S1). Specifically, AN (80.5°N, 94.8°E) is located ∼5,000 km from Melle, ∼4,200 km from the mining sites in Derbyshire (England), and ∼4,300 km from the Harz Mountains sites. Similarly, NGRIP (75.1°N, 42.3°W) is located ∼3,800 km from Melle, ∼2,900 km from the Derbyshire sites, and ∼3,500 km from the Harz Mountains sites.

To assess the likely sources of pollution lead measured in the Arctic ice core array, and lacking the detailed meteorological data necessary for modeling transport during ancient times, we used 1920 to 1999 CE backward simulations with the state-of-the-art FLEXPART atmospheric aerosol transport and deposition model (18, 19), on the assumption that atmospheric transport was similar during the past 2,200 y. In addition to AN, simulations were used to determine average emissions sensitivity fields for the NGRIP (2), NEEM, Tunu, Summit, and ACT2 core sites, each assumed to be representative of the north central, northwest, northeast, central, and southwest regions of the Greenland ice sheet, respectively (Fig. 1 and *SI Appendix*, Figs. S3 and S4). The magnitude of the emissions sensitivity depends heavily on the scavenging properties of the aerosol and the precipitation input used by FLEXPART, so it may be subject to systematic biases in the model. To test sensitivity of the results to the assumed ambient aerosol type, we performed separate calculations for 4 different aerosol types: mineral dust with logarithmic mean diameters of 1 μm (SD 0.9) and 5 μm (SD 0.9), as well as sulfate and black carbon aerosols with assumed logarithmic mean diameters of 0.4 μm (SD of 0.3). However, lead attaches to ambient background aerosol which may preexist in the atmosphere or be comobilized with lead, so, consistent with previous studies (2), we assumed that the lead aerosol consisted mainly of the smaller 1-μm mineral dust. Based on differences between the 4 different model tracers, we estimated an uncertainty in the overall magnitude of the lead emissions sensitivity to be a factor of 2.

ACKNOWLEDGMENTS. Collection, analysis, and interpretation of the ice cores in the Arctic array were supported by grants from the National Science Foundation (0216552, 0421412, 0221515, 0856845, 0909541, 1023672, 1406219, and 1406236); NASA (NAG04GI66G); the John Fell Oxford University Press Research Fund and All Souls College, Oxford; and DRI. We thank the Alfred Wegener Institute, the NGRIP and NEEM community, and other field personnel for assistance in drilling the ice cores (K. Steffen); and students and staff, including O. Maselli, D. Pasteris, and M. Sigl, in the DRI ice core group for assistance in the field and laboratory.

1. S. Hong, J. P. Candelone, C. C. Patterson, C. F. Boutron, Greenland ice evidence of hemispheric lead pollution two millennia ago by Greek and Roman civilizations. *Science* **265**, 1841–1843 (1994).
2. J. R. McConnell *et al*., Lead pollution recorded in Greenland ice indicates European emissions tracked plagues, wars, and imperial expansion during antiquity. *Proc. Natl. Acad. Sci. U.S.A.* **115**, 5726–5731 (2018).
3. J. R. McConnell, G. W. Lamorey, M. A. Hutterli, A 250-year high-resolution record of Pb flux and crustal enrichment in central Greenland. *Geophys. Res. Lett.* **29**, 2130–2132 (2002).
4. J. R. McConnell, R. Edwards, Coal burning leaves toxic heavy metal legacy in the Arctic. *Proc. Natl. Acad. Sci. U.S.A.* **105**, 12140–12144 (2008).
5. J. P. Candelone, S. M. Hong, C. Pellone, C. F. Boutron, Post-industrial revolution changes in large-scale atmospheric pollution of the Northern Hemisphere by heavy metals as documented in central Greenland snow and ice. *J. Geophys. Res.* **100**, 16605–16616 (1995).
6. K. Rosman, W. Chisholm, S. Hong, J. Candelone, C. Boutron, Lead from Carthaginian and Roman Spanish mines isotopically identified in Greenland ice dated from 600 BC to 300 AD. *Environ. Sci. Technol.* **31**, 3413–3416 (1997).
7. A. F. More *et al*., Next-generation ice core technology reveals true minimum natural levels of lead (Pb) in the atmosphere: Insights from the Black Death. *GeoHealth* **1**, 211–219 (2017).
8. C. P. Loveluck *et al*., Alpine ice-core evidence for the transformation of the European monetary system, AD 640-670. *Antiquity* **92**, 1571–1585 (2018).
9. S. Preunkert *et al*., Lead and antimony in basal ice from Col du Dome (French Alps) dated with radiocarbon: A record of pollution during antiquity. *Geophys. Res. Lett.* **46**, 4953–4961 (2019).
10. J. Nriagu, Paleoenvironmental research–Tales told in lead. *Science* **281**, 1622–1623 (1998).
11. J. Esper *et al*., Environmental drivers of historical grain price variations in Europe. *Clim. Res.* **72**, 39–52 (2017).
12. F. Ljungqvist *et al*., Linking European building activity with plague history. *J. Archaeol. Sci.* **98**, 81–92 (2018).
13. J. R. McConnell *et al*., Synchronous volcanic eruptions and abrupt climate change ∼17.7 ka plausibly linked by stratospheric ozone depletion. *Proc. Natl. Acad. Sci. U.S.A.* **114**, 10035–10040 (2017).
14. J. R. McConnell, G. W. Lamorey, S. W. Lambert, K. C. Taylor, Continuous ice-core chemical analyses using inductively coupled plasma mass spectrometry. *Environ. Sci. Technol.* **36**, 7–11 (2002).
15. W. Shotyk *et al*., History of atmospheric lead deposition since 12,370 ^{14}C yr BP from a peat bog, Jura Mountains, Switzerland. *Science* **281**, 1635–1640 (1998).
16. M. Brannvall *et al*., The Medieval metal industry was the cradle of modern large scale atmospheric lead pollution in northern Europe. *Environ. Sci. Technol.* **33**, 4391–4395 (1999).
17. R. Bindler, Comment on "next-generation ice core technology reveals true minimum natural levels of lead (Pb) in the atmosphere: Insights from the Black Death" by More et al. *GeoHealth* **2**, 155–161 (2018).
18. S. Eckhardt *et al*., Source-receptor matrix calculation for deposited mass with the Lagrangian particle dispersion model FLEXPART v10.2 in backward mode. *Geophys Model Dev* **10**, 4605–4618 (2017).
19. A. Stohl, C. Forster, A. Frank, P. Seibert, G. Wotawa, Technical note: The Lagrangian particle dispersion model FLEXPART version 6.2. *Atmos. Chem. Phys.* **5**, 2461–2474 (2005).
20. A. L. Hillman, M. B. Abbott, J. Yu, D. J. Bain, T. Chiou-Peng, Environmental legacy of copper metallurgy and Mongol silver smelting recorded in Yunnan Lake sediments. *Environ. Sci. Technol.* **49**, 3349–3357 (2015).
21. E. Liu *et al*., Historical reconstruction of atmospheric lead pollution in central Yunnan province, southwest China: An analysis based on lacustrine sedimentary records. *Environ. Sci. Pollut. Res. Int.* **20**, 8739–8750 (2013).
22. F. Téreygeol, How to quantify medieval silver production at Melle? *Metalla* **20**, 59–86 (2013).
23. U. Büntgen *et al*., 2500 years of European climate variability and human susceptibility. *Science* **331**, 578–582 (2011).
24. I. Blanchard, "Mining, Metallurgy and Minting in the Middle Ages" in *Asiatic Supremacy 425–1125* (Franz Steiner Verlag, Stuttgart, Germany, 2001), vol. 1, p. 550.
25. I. Blanchard, "Mining, Metallurgy and Minting in the Middle Ages" in *Afro-European Supremacy 1125–1225* (Franz Steiner Verlag, Stuttgart, Germany, 2001), vol. 2, p. 366.
26. I. Blanchard, "Mining, Metallurgy and Minting in the Middle Ages" in *Continuing Afro-European Supremacy, 1250–1450* (Franz Steiner Verlag, Stuttgart, Germany, 2001), vol. 3, p. 786.
27. J. U. Nef, Silver production in Central Europe, 1450-1618. *J. Polit. Econ.* **49**, 575–591 (1941).
28. G. Agricola, *De Re Metallica* (1556), trans H. C. Hoover and L. C. Hoover (Dover Publications, Mineola, NY, 1950).
29. U. Büntgen, C. Ginzler, J. Esper, W. Tegel, A. J. McMichael, Digitizing historical plague. *Clin. Infect. Dis.* **55**, 1586–1588 (2012).
30. J. H. Rieuwerts, Early gunpowder work in Longe or Cromford Sough, Derbyshire, 1662-1663 and 1676-1680. *Minn. Hist.* **13**, 1–5 (1998).
31. R. J. Evans, Epidemics and revolutions: Cholera in nineteenth-century Europe. *Past Present* **120**, 123–146 (1988).
32. H. Berger, M. Spoerer, Economic crises and the European revolutions of 1848. *J. Econ. Hist.* **61**, 293–326 (2001).
33. A. Vinogradova, Distant evaluation of the influence of air pollution on remote areas. *Izv. Atmos. Ocean. Phys.* **51**, 712–722 (2015).
34. V. Shevchenko, A. Lisitzin, A. Vinogradova, R. Stein, Heavy metals in aerosols over the seas of the Russian Arctic. *Sci. Total Environ.* **306**, 11–25 (2003).
35. T. Opel, D. Fritzsche, H. Meyer, Eurasian Arctic climate over the past millennium as recorded in the Akademii Nauk ice core (Severnaya Zemlya). *Clim. Past* **9**, 2379–2389 (2013).
36. M. M. Arienzo, J. R. McConnell, N. Chellman, S. Kipfstuhl, Method for correcting continuous ice-core elemental measurements for under-recovery. *Environ. Sci. Technol.* **53**, 5887–5894 (2019).
37. M. Sigl *et al*., Insights from Antarctica on volcanic forcing during the Common Era. *Nat. Clim. Chang.* **4**, 693–697 (2014).
38. M. Sigl *et al*., Timing and climate forcing of volcanic eruptions for the past 2,500 years. *Nature* **523**, 543–549 (2015).
39. F. Adolphi, R. Muscheler, Synchronizing the Greenland ice core and radiocarbon timescales over the Holocene – Bayesian wiggle-matching of cosmogenic radionuclide records. *Clim. Past* **12**, 15–30 (2016).
40. M. M. Arienzo *et al*., A method for continuous (239)Pu determinations in Arctic and Antarctic ice cores. *Environ. Sci. Technol.* **50**, 7066–7073 (2016).
41. J. Luterbacher *et al*., European summer temperatures since Roman times. *Environ. Res. Lett.* **11**, 024001 (2016).